Neuron
Article

Dendrite Self-Avoidance Requires Cell-Autonomous Slit/Robo Signaling in Cerebellar Purkinje Cells

Daniel A. Gibson,[1,2] Stephen Tymanskyj,[1] Rachel C. Yuan,[1,2] Haiwen C. Leung,[1] Julie L. Lefebvre,[4] Joshua R. Sanes,[4] Alain Chédotal,[5] and Le Ma[1,2,3,*]
[1]Zilkha Neurogenetic Institute
[2]Neuroscience Graduate Program
[3]Department of Cell and Neurobiology
Keck School of Medicine, University of Southern California, Los Angeles, CA 90089, USA
[4]Center for Brain Science and Department of Molecular and Cellular Biology, Harvard University, Cambridge, MA 02138, USA
[5]Sorbonne Universités, UPMC Univ Paris 06, INSERM UMR_S968, CNRS_UMR7210, Institut de la Vision, 750012, Paris, France
*Correspondence: le.ma@usc.edu
http://dx.doi.org/10.1016/j.neuron.2014.01.009

SUMMARY

Dendrites from the same neuron usually develop nonoverlapping patterns by self-avoidance, a process requiring contact-dependent recognition and repulsion. Recent studies have implicated homophilic interactions of cell surface molecules, including Dscams and Pcdhgs, in self-recognition, but repulsive molecular mechanisms remain obscure. Here, we report a role for the secreted molecule Slit2 and its receptor Robo2 in self-avoidance of cerebellar Purkinje cells (PCs). Both molecules are highly expressed by PCs, and their deletion leads to excessive dendrite self-crossing without affecting arbor size and shape. This cell-autonomous function is supported by the boundary-establishing activity of Slit in culture and the phenotype rescue by membrane-associated Slit2 activities. Furthermore, genetic studies show that they act independently from Pcdhg-mediated recognition. Finally, PC-specific deletion of Robo2 is associated with motor behavior alterations. Thus, our study uncovers a local repulsive mechanism required for self-avoidance and demonstrates the molecular complexity at the cell surface in dendritic patterning.

INTRODUCTION

Dendrites are the sites of synaptic inputs and often grow in nonoverlapping patterns that maximize receptive field coverage while minimizing redundant inputs (Jan and Jan, 2010). Development of such a pattern in single neurons is achieved by self-avoidance, an active process involving contact-dependent recognition and repulsion between neighboring sister branches (Grueber and Sagasti, 2010).

Initially discovered in leech mechanosensory neurons (Kramer and Kuwada, 1983), self-avoidance has been found for both axons and dendrites in a wide range of invertebrate and vertebrate neurons (Fujishima et al., 2012; Hughes et al., 2007; Liu and Halloran, 2005; Matthews et al., 2007; Montague and Friedlander, 1991; Sagasti et al., 2005; Sdrulla and Linden, 2006; Soba et al., 2007). Recent invertebrate studies have identified a number of cell-surface molecules that are required cell-autonomously for establishing nonoverlapping dendrites or axons in an approximately two-dimensional (2D) plane. They include the Down syndrome cell adhesion molecule (Dscam) (Hughes et al., 2007; Matthews et al., 2007; Soba et al., 2007), the secreted guidance molecule Netrin and its receptors (Smith et al., 2012), the cadherin member Flamingo (Fmi) (Matsubara et al., 2011), the leukocyte antigen-related (LAR) protein receptor tyrosine phosphatase (Baker and Macagno, 2000), the cell adhesion molecule integrin (Han et al., 2012; Kim et al., 2012), and the tripartite ligand-receptor complex involving SAX-7, MNR-1, and DMA-1 (Dong et al., 2013; Salzberg et al., 2013). In mammals, however, only a few molecules, including Dscam and the related DscamL1 (Fuerst et al., 2009), the transmembrane semaphorin 6A (Sema6A) (Matsuoka et al., 2012), and the gamma cluster of protocadherins (Pcdhgs) (Lefebvre et al., 2012), have been studied for their self-avoidance function in subpopulations of retinal cells and cerebellar Purkinje cells (PCs).

Recent investigation of several cell surface molecules has drawn attention to the mechanisms involved in recognition. Studies of *Drosophila* Dscams (Wojtowicz et al., 2004, 2007) and mammalian Pcdhgs (Chen et al., 2012; Lefebvre et al., 2012; Yagi, 2008) pointed to a novel mechanism involving diverse isoforms generated by alternative splicing or promoter usage for these molecules. Homophilic interaction of specific isoforms at the branch surface confers unique molecular identities on each neuron and thus promotes the distinction between "self" and "nonself" (Zipursky and Sanes, 2010). Interestingly, in *Caenorhabditis elegans*, the secreted molecule Netrin/UNC-6 was also proposed to mediate recognition, but via a capture-and-display mechanism involving two distinct receptors expressed on neighboring dendrites (Smith et al., 2012). In both cases, the molecular interaction fits well with the contact-dependent nature of self-avoidance as revealed by live imaging (Fujishima et al., 2012; Liu and Halloran, 2005; Montague and Friedlander, 1991; Sagasti et al., 2005; Sdrulla and Linden, 2006; Smith et al., 2012).

Despite the current progress in recognition, mechanisms involved in other aspects of self-avoidance, such as repulsion, remain poorly understood (Grueber and Sagasti, 2010). Although two axon guidance cues, Netrin and Sema6A, were recently implicated (Matsuoka et al., 2012; Smith et al., 2012), it is not clear whether repulsive molecules in general can promote self-avoidance. In addition, it is not clear whether mechanisms involved in repulsion cooperate with recognition or function independently. Furthermore, nearly all the molecular mechanisms identified so far involve interactions between transmembrane proteins (Grueber and Sagasti, 2010), and the role of secreted factors in mediating self-avoidance is not clear.

In this study, we analyze the function of the secreted repulsive guidance cues Slits and their cognate Robo receptors during cerebellar PC development. Slits are a family of secreted proteins (Slit1-3 in mammals) that often act as repulsive cues to regulate axon guidance, cell migration, and other developmental processes (Borrell et al., 2012; Domyan et al., 2013; Giovannone et al., 2012; Grieshammer et al., 2004; Long et al., 2004; Ma and Tessier-Lavigne, 2007; Wang et al., 2013; Wu et al., 2001). Slit functions are primarily mediated by two transmembrane proteins Robo1 and Robo2 (Bashaw and Klein, 2010; Chédotal, 2007). Here, we show that both *Slit2* and *Robo2* are highly expressed by PCs during dendritic arbor development and are required cell-autonomously for self-avoidance. Further analysis indicates that Slit proteins can repel PC dendrites in vitro and need to be localized to the dendritic surface in vivo. Furthermore, we demonstrate genetically that Slit/Robo and Pcdhgs act in separate extracellular pathways and provide first evidence to link defective self-avoidance and changes in animal behavior. Thus, our study identifies another molecular system required for self-avoidance in a mammalian neuron and suggests that complex arbors may require multiple mechanisms to achieve mature morphology.

RESULTS

Robo2 Is Expressed in PC Dendrites during Dendritic Growth

In rodents, PC dendritic arbors undergo rapid expansion during the second and third postnatal week when extensive new branches are added (McKay and Turner, 2005). Previous studies have shown PC-specific expression of *Robo2*, but not *Robo1*, in adult mice (Lein et al., 2007) and in embryonic through adult rat cerebellum (Marillat et al., 2002). We confirmed this pattern by performing RNA in situ hybridization during PC dendritogenesis at postnatal day (P) 14. At this age, *Robo2* mRNA is strongly expressed in PC somas in the PC layer (PCL) (Figure 1B), which is apparent in a high-magnification view (Figure 1C). *Robo2* mRNA is only present at background levels in the granule cell layer (GCL) and is notably absent from molecular layer (ML) neurons (Figure 1C). As a comparison, *Robo1* transcripts were not detected in PCs (Figure 1A), suggesting that Robo2 is the main receptor expressed during PC dendritogenesis.

We also examined Robo2 protein localization in P21 cerebella by immunostaining using a Robo2-specific antibody (Figures 1D–1F). The immunostaining signal was found in both dendrites and somas of wild-type PCs (Figure 1E) and colocalized with the PC-marker, Calbindin (Figures 1D and 1F). To demonstrate the specificity of the antibody, we examined the staining in the cerebellum carrying a PC-specific Cre driver (*Pcp2-Cre* or *L7-Cre*) and conditional *Robo2* alleles ($Robo2^{flox/flox}$) (Figures 1G–1I) (Barski et al., 2000; Lu et al., 2007). Deletion of the loxP-flanked exon 5 in *Robo2* results in unstable Robo2 proteins (Lu et al., 2007) and hence the loss of immunostaining signal in PCs (Figure 1H). Furthermore, Robo2 staining is absent from the wild-type PC axons (data not shown), suggesting dendrite-specific expression. Taken together, the expression of Robo2 during PC dendritogenesis suggests its potential role in self-avoidance or other processes that contribute to proper dendrite patterning.

Deletion of Robo2 Leads to Self-Crossing of PC Dendrites

To investigate the function of Robo2 in dendritic development of individual PCs, we adopted a mosaic analysis method by injecting recombinant adeno-associated virus (rAAV) into the cerebellar midline of $Robo2^{flox/flox}$ mice on the day of birth (P0) (Gibson and Ma, 2011). This approach allowed us to selectively delete *Robo2* in single PCs and visualize the entire dendritic arbor. The $Robo2^{flox}$ allele was used because it had been used to recapitulate the kidney and urinary tract defects (Lu et al., 2007) and the sensory axon overshooting defect (Figures S1A and S1B available online) found with a *Robo2* null allele (Grieshammer et al., 2004; Ma and Tessier-Lavigne, 2007). We chose to use rAAV8 because this serotype infects only PCs in the cerebellum (Pilpel et al., 2009). A mixture of rAAV8 expressing either DsRed (AAV-DsRed) or coexpressing Cre and GFP from separate promoters (AAV-Cre-GFP) was used to produce a sparse in vivo mosaic of control ($DsRed^+$) or Robo2-deficient (GFP^+) PCs. At the concentrations used, PCs were rarely coinfected by both viruses, thereby exhibiting mutually exclusive DsRed and GFP expression (Figure S1F). GFP and DsRed labeling perfectly overlaps when the two viruses are coexpressed (data not shown) and GFP^+ cells have consistent Cre activities as demonstrated by the tdTomato reporter (Figures S1–S1E) or the loss of Robo2 immunostaining (Figure S1G). Thus this experimental design provides a reliable and unbiased means to compare control and mutant PCs in the same cerebellum.

We analyzed PC dendrites at P21 when they have developed nearly mature arbor morphology. Single-labeled PCs throughout the cerebellum were imaged by confocal microscopy and then traced and reconstructed in three-dimensions (3D) from thin optical sections (<0.75 μm) using Neurolucida. $DsRed^+$ control PC arbors consisted of smooth primary dendrites and many spiny secondary branches restricted to and arborizing within the ML (Figures 2A–2C). They showed a strong tendency of self-avoidance with few crosses of sister dendrites in the projected reconstructions (Figures 2B and 2C). In contrast, tracing of GFP^+ *Robo2* mutant PCs revealed extensive overlapping of sister branches (Figures 2D–2F). The overlaps were observed throughout the tree, but only between the high-order spiny branches and not between smooth primary dendrites (Figures 2A and 2D, arrowheads). For comparison, this crossing defect was not seen in wild-type neurons infected by AAV-Cre-GFP (Figures S1H and S1I).

To quantify the crosses observed in control and *Robo2* mutant PCs, we developed an unbiased sampling method by analyzing

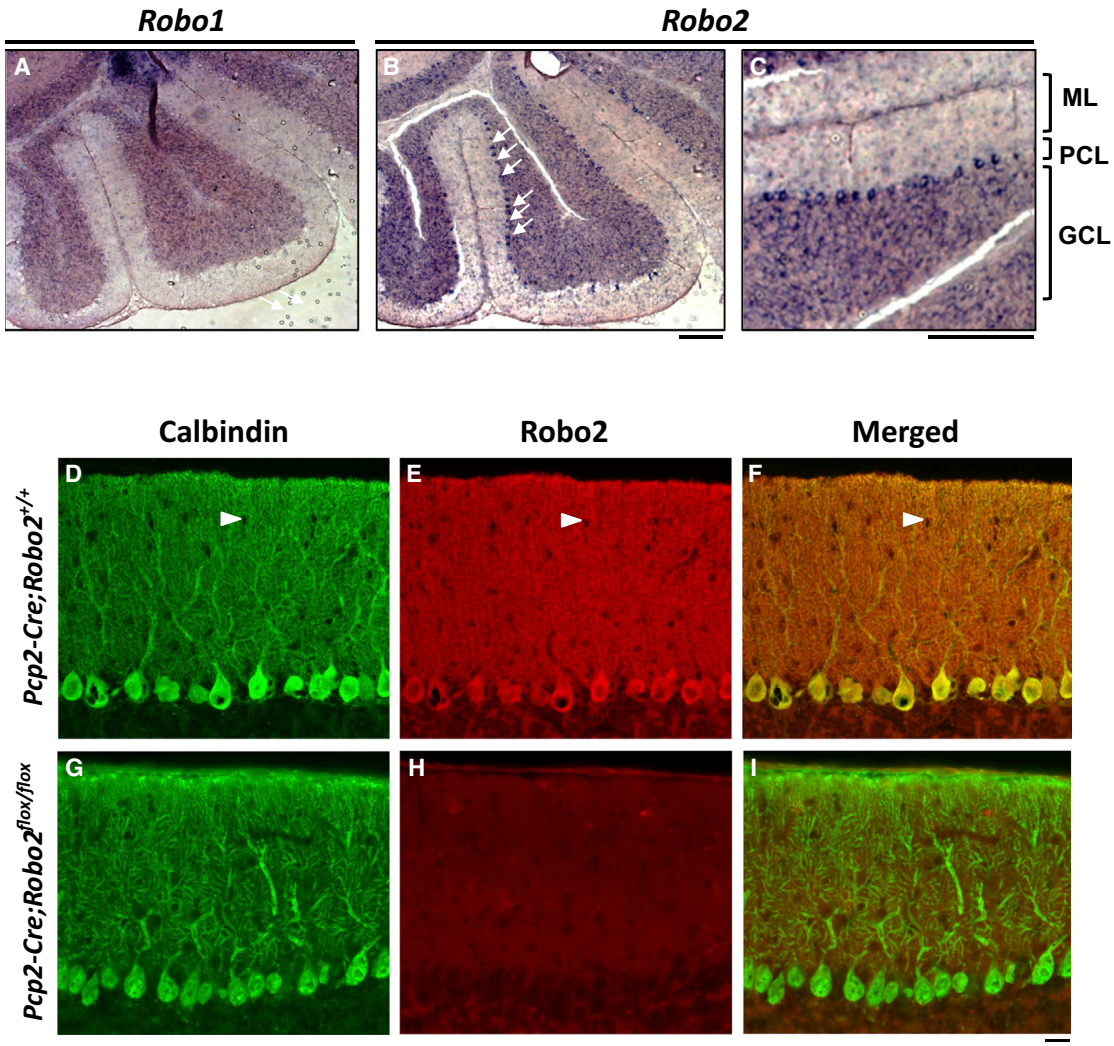

Figure 1. Robo2 Is Expressed by Purkinje Cells

(A–C) In situ hybridization of *Robo1*(A) and *Robo2* (B) in P14 cerebellum. ML, PCL, and GCL are shown in a high-magnification region of the cerebellum for *Robo2* (C). Arrows indicate PC somas. Scale bars represent 100 μm.

(D–I) Sections of P21 cerebellum from animals carrying both a *Pcp2-Cre* driver and $Robo2^{+/+}$ (D and F) or $Robo2^{flox/flox}$ (G–I) alleles were stained with antibodies for Calbindin (D and G) or Robo2 (E and H). In the merged image of the *Pcp2-Cre* ;$Robo2^{+/+}$ section (F), the red Robo2 signal is similar to the green Calbindin staining in the cell body and primary dendrites, giving yellowing appearance, whereas it is much stronger on the spiny dendrites, making the entire ML reddish. In the *Pcp2-Cre*;$Robo2^{flox/flox}$ section, Robo2 immunostaining was undetectable (H), resulting in an ML labeled mostly with the green Calbindin staining label in the merged image (I). Note, interneuron cell bodies were not labeled and appeared as black holes (arrows heads, D–F). Scale bar represents 20 μm (D–I).

See also Figure S1.

randomly selected 100 μm^2 regions (Figures S2A and S2B), which altogether cover ~20% of each arbor. Using this analysis, we found that $DsRed^+$ control PCs have only 0.8 ± 0.2 crosses per 100 μm of dendrite length whereas GFP^+ *Robo2* mutant PCs have a significantly higher frequency of self-crossing with 6.1 ± 0.5/100 μm (Figure 2J). We also confirmed this result by analyzing the complete reconstruction of PC dendritic arbors, which showed a nearly identical difference between control and mutant PCs (Figures S2C and S2D), thus validating the sampling method. Furthermore, in mice carrying the homozygous $Robo1^{-/-}$ null alleles (Long et al., 2004) and the $Robo2^{flox/flox}$ or $Robo2^{-/flox}$ alleles, simultaneously deleting *Robo1* and *Robo2* by AAV-Cre-GFP led to excessive PC dendritic crosses (4.1 ± 0.5/100 μm; n = 7; Figures S2E–S2H) with a frequency similar to that in single *Robo2* knockout PCs, whereas Robo1 only deletion as labeled by AAV-DsRed had the control-level of crosses (0.9 ± 0.04/100 μm, n = 7). These results suggest that Robo2 is the primary receptor required for PC arbor patterning.

Deletion of Robo2 in PCs Only Affects Dendrite Self-Avoidance

To rule out that the self-crossing phenotype is secondary to other defects in dendritic development, we further characterized

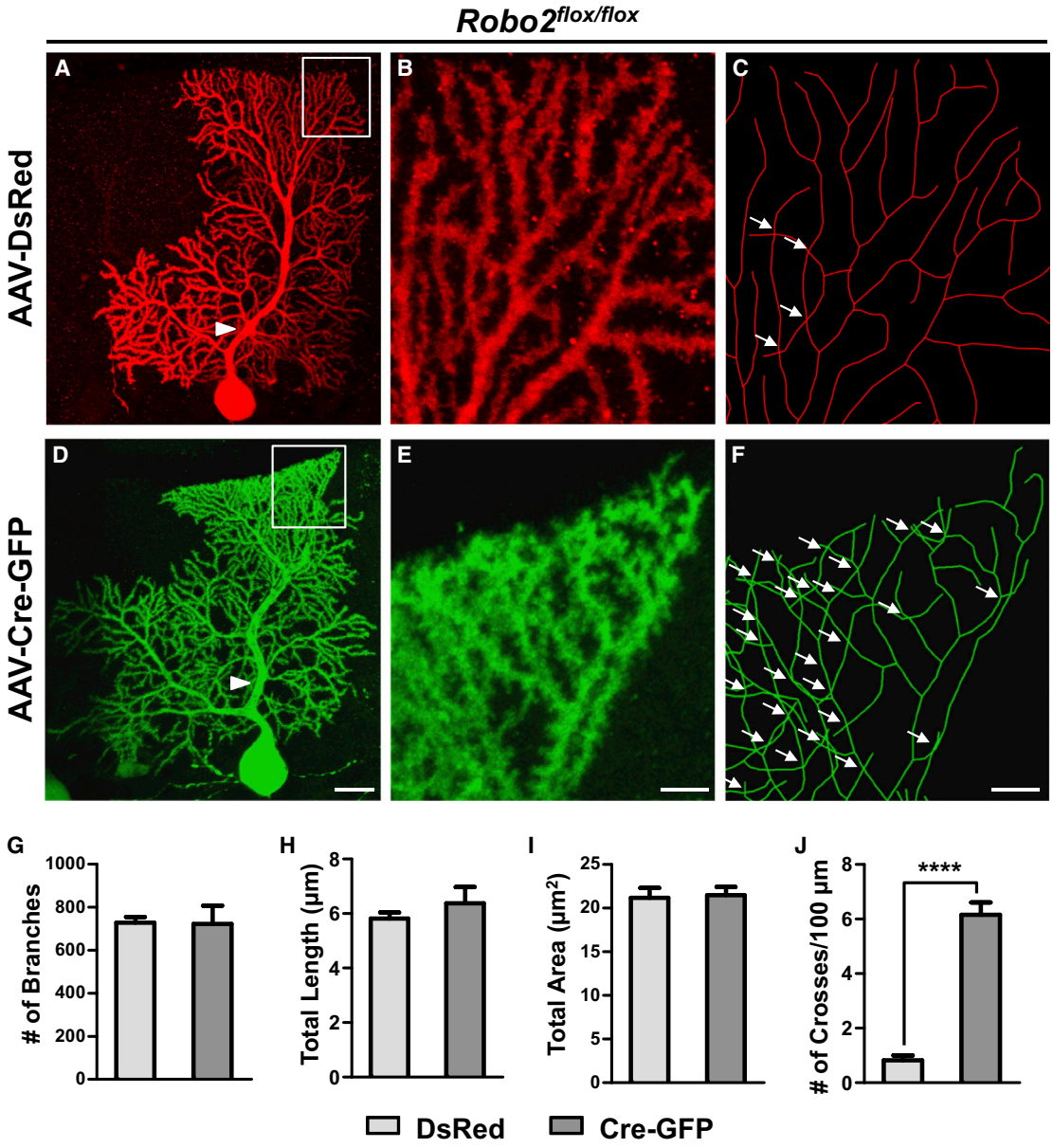

Figure 2. Robo2 Is Required for PC Dendrite Self-Avoidance

(A–F) *Robo2*$^{flox/flox}$ PCs infected with AAV-DsRed (A–C) or AAV-Cre-GFP (D–F) are shown by z projections of confocal images (A, B, D, and E) or skeletonized reconstructions (C and F). High-magnification images shown in (B, C, E, and F) correspond to the respective boxed regions in (A and D). Arrowheads point to smooth primary dendrites, while arrows indicate self-crosses. Scale bars represent 100 μm (A and D); 5 μm (B, C, E, and F).

(G–J) Quantification of the number (#) of branches (G), the total dendrite length (H), the total area of the dendritic arbor (I), and the frequency of self-crossing expressed as the number (#) of crosses per 100 μm of dendrite length (J) of labeled PCs (G–I, n = 5 cells, three mice; J, n = 12 cells, five mice, ****p < 0.0001, Student's t test). Data are shown by mean ± SEM.

See also Figure S2.

the dendritic morphology in *Robo2*-deleted PCs. Using measurements from 3D reconstructions, we found no significant changes in other dendrite properties, such as total dendrite length, number of branches, or total dendritic area (Figures 2G–2I). Nor was there any correlation of the defect with any particular arbor shape (data not shown), indicating that the defect applies to all PCs. Furthermore, individual *Robo2* mutant PCs showed no changes in monoplanarity (data not shown) or spine development (see below, Figure S5). When *Robo2* was deleted from all PCs using the *Pcp2-Cre* driver (Barski et al., 2000), no other gross aspects of neural development were altered (see below, Figure S5), except that the same crossing defect was apparent in PCs sparsely labeled by AAV-DsRed (Figure S5A). Thus, loss of *Robo2* in PCs specifically perturbs

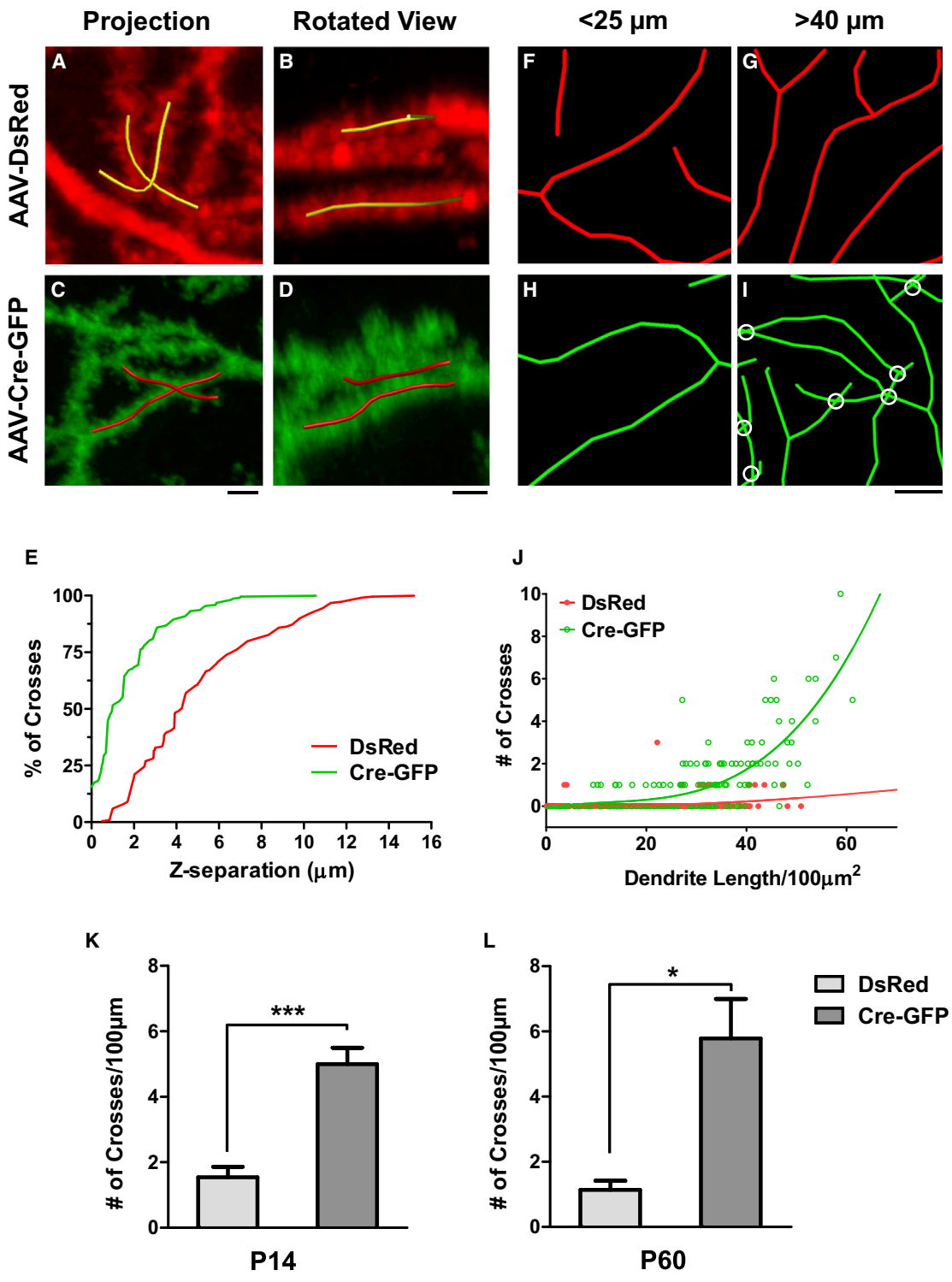

Figure 3. Robo2 Is Required for an Active Local Avoidance Mechanism

(A–D) Z projections of confocal images (A and C) with the accompanying rotated views (B and D) of single self-crosses from AAV-DsRed-labeled control (A and B) and AAV-Cre-GFP-infected mutant (C and D) *Robo2*$^{flox/flox}$ PCs. Yellow (A and B) and red (C and D) lines are reconstructed portions of crossing branches; untraced branches are in the background in the rotated views (B and D) and are not part of the indicated self-crossing. Scale bars represent 2 µm.

(E) A cumulative frequency distribution plot illustrates the percentage of self-crosses that occur within a given distance along the z axis for control (red line) and mutant (green line) PCs.

(legend continued on next page)

the spacing of neighboring branches, a hallmark of impaired self-avoidance.

We further investigated the phenotype by analyzing the distance between crossing branches along the z axis using 3D reconstructions. We reasoned that an impairment of self-avoidance would result in crossing branches that are in closer proximity to each other than the few crosses observed in control cells in which self-avoidance mechanisms are intact. Indeed, the rare self-crosses in control cells were separated along the z axis (Figures 3A and 3B) with a median separation of ~4 μm (Figure 3E). In contrast, over 50% of the self-crosses found in the GFP$^+$ PCs (Figures 3C and 3D) were between branches passing within 1 μm of each other. As a comparison, <6% of crosses in control cells were within this distance (Figure 3E). The reduced spacing between crossing branches along the z axis further suggests that the defect is due to the loss of a short-range spacing mechanism in mutant PCs, consistent with a role of Robo2 in self-avoidance.

We also analyzed the crossing data collected from the sampling method and plotted the relationship between the number of self-crosses and dendritic density (total dendrite length/100 μm^2). In *Robo2* mutant PC arbors, the number of self-crosses rapidly increased along with dendritic density (Figures 3H–3J). In contrast, control PC arbors did not show this correlation at all (Figures 3F, 3G, and 3J), suggesting that a normally active self-avoidance mechanism is impaired in *Robo2* mutant cells.

To assess the time course of normal self-avoidance and the effect of *Robo2* deletion, we repeated our neonatal virus injection in P0 *Robo2*$^{flox/flox}$ pups and analyzed PCs at two additional ages, P14 and P60. At both ages, we found that DsRed$^+$ control PCs exhibited a low frequency of self-crossing, whereas GFP$^+$ mutant PCs displayed a high frequency (Figures 3K and 3L versus Figure 2J). These results indicate that the defect produced by *Robo2* deletion occurs early in development and is not corrected over the time period analyzed.

Expression of Slit Genes in PCs

Given the role of Robo2 in self-avoidance, we asked whether any of the known Slit ligands are required by first investigating the expression of *Slit1-3* in P14 cerebella. By in situ hybridization, *Slit2* mRNA was found exclusively in PC cell bodies (Figures 4A and 4B). *Slit1* and *Slit3* mRNAs were primarily restricted to the GCL (Figures S3A–S3C), as shown previously in the rat cerebellum (Marillat et al., 2002). In addition, *Slit1* is weakly expressed by a subset of PCs (Figure S3B).

We next probed P14 mouse cerebellar samples for the presence of Slit2 protein by western blot. Isolated cerebellar tissues were processed as a whole cerebellum lysate or further microdissected to separate the GCL from ML and PCL to assess the laminar distribution of proteins. By probing these samples with a specific antibody, we found Slit2 enriched in ML+PCL relative to GCL (Figure 4C). This result suggests that, like Robo2, Slit2 gene expression is restricted to PCs and the protein appears to be predominant in the ML, most likely in PC dendrites. This finding is intriguing, because it suggests that the ligand might also be required cell-autonomously for PC dendrite development.

Deletion of Slits from PCs Also Leads to Dendrite Self-Crossing

To test for the cell-autonomous role of Slit2 in self-avoidance, we next examined the consequence of a PC-specific *Slit2* deletion. We injected neonatal pups homozygous for a *Slit2*^{flox} allele with a combination of AAV-DsRed and AAV-Cre-GFP as described above (Figures 4D–4I). In these animals, DsRed$^+$ control PCs displayed a low frequency of self-crossing at a level (1.0 ± 0.1/100 μm) similar to control *Robo2*$^{flox/flox}$ PCs (Figure 4J versus Figure 2J). The frequency of self-crossing in GFP$^+$ *Slit2* mutant PCs, however, was significantly higher (5.4 ± 0.5/100 μm) and increased by ~5-fold relative to control cells and reached a level equivalent to that of *Robo2* mutant PCs (Figure 4J versus Figure 2J). This is consistent with the known interactions between this ligand/receptor pair (Chédotal, 2007) and suggests that their repulsive function might mediate PC self-avoidance. Additionally, the phenotypic similarity and the PC-specific expression of Slit2 and Robo2 suggest that the ligand acts in an autocrine fashion.

We also examined PCs in mice homozygous for a *Slit1* null allele (Plump et al., 2002) because some PCs weakly express *Slit1* (Figures S3A and S3B). Based on AAV-DsRed labeling of mutant and control littermates, we observed that PCs in *Slit1* mutant animals exhibited an increase in self-crossing frequency of ~4-fold (4.5 ± 0.8/100 μm) relative to control PCs (1.0 ± 0.1/100 μm) (Figure S3D). Thus, *Slit1* is also required for PC dendrite self-avoidance. Its expression in both PCL and GCL and the lack of a conditional allele, however, preclude the determination of its cell-autonomous or non-cell-autonomous action.

PC Dendrites Fail to Cross a Slit-Boundary in Explant Cocultures

Slit2 expressed by PCs may associate with dendrites and serve as repulsive barriers to sister branches (Fujishima et al., 2012; Sdrulla and Linden, 2006). Thus, we asked whether Slit proteins could repel PC dendrites. We developed an organotypic culture using foliar explants isolated from P7 mouse cerebella and culturing them next to COS cell aggregates (Figure 5A). Normally, after ~10 days in vitro (DIV), some PC dendrites located at the edge of isolated explants extended toward the periphery and away from the majority of other PCs in the explant, as shown by the staining of the PC marker, Calbindin.

(F–I) Examples of reconstructed dendritic branches in AAV-DsRed infected control (F and G) and AAV-Cre-GFP infected mutant (H and I) *Robo2*$^{flox/flox}$ PCs from a fixed area (100 μm^2) with both short (F and H) and long (G and I) total dendrite lengths. Scale bar represents 2 μm.

(J) Plot of the relationship between the total dendrite length in a fixed area and the number of self-crosses in control (red line and dots) and mutant (green line and dots) PCs. Solid lines are lines of best fit.

(K–L) The frequency of self-crossing is quantified as the number (#, mean ± SEM) of crosses per 100 μm for AAV-DsRed- or AAV-Cre-GFP-infected PCs analyzed at P14 (K, n = 5 cells, three mice) or P60 (L, n = 5 DsRed cells or 6 Cre-GFP cells, three mice). *p < 0.05 and ***p < 0.001, Student's t test.

See also Figure S3.

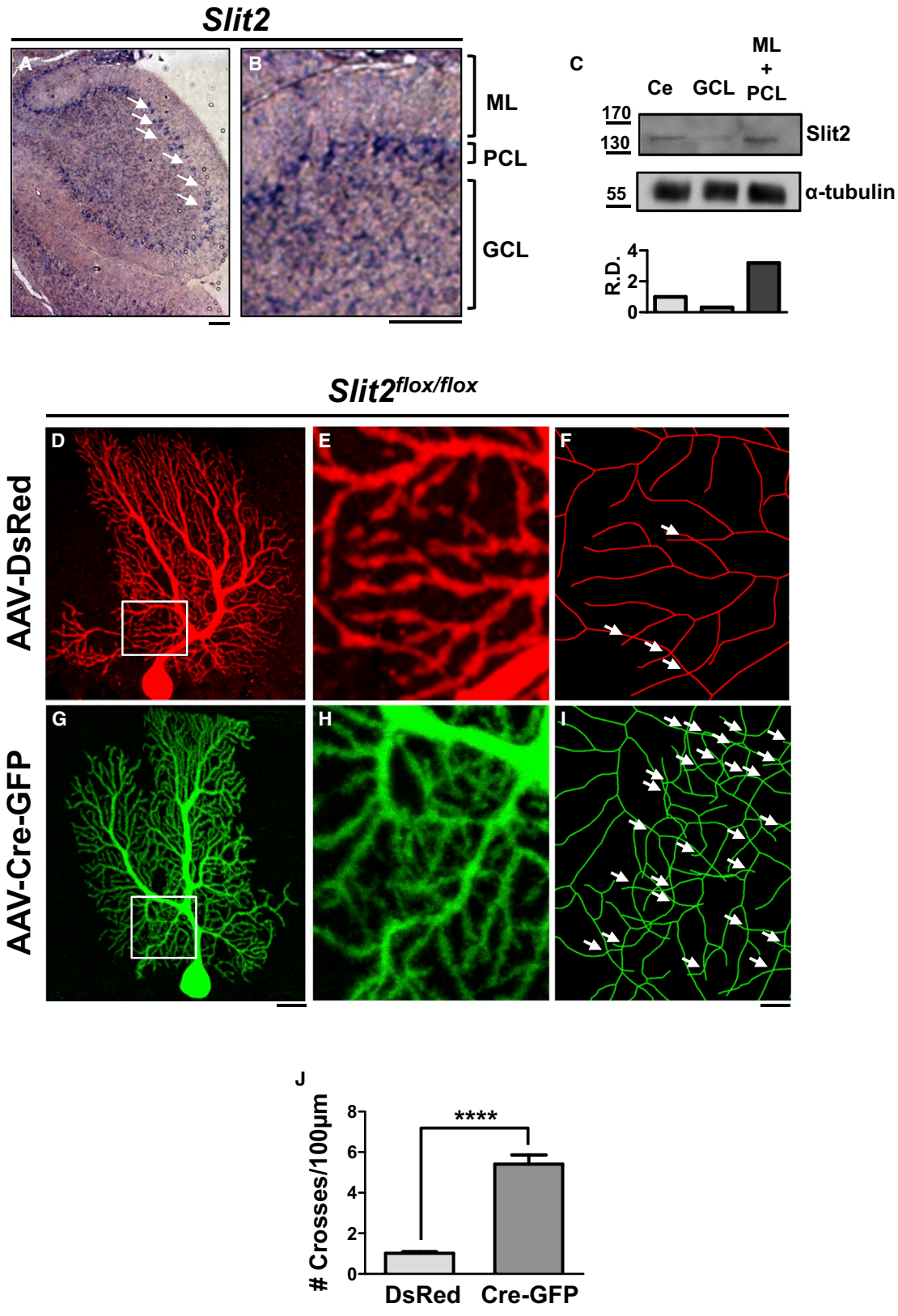

(legend on next page)

When mock-transfected control COS cell aggregates were placed adjacent to the explant at this time point and then cultured for an additional 3 DIV, PC dendrites freely crossed the boundary identified from DIC images or by nuclear staining and grew to some distance (Figure 5B). In contrast, when COS cell aggregates expressing full-length Slit1 and Slit2 were placed adjacent to the explant, PC dendrites in about half of the explants failed to cross the explant-aggregate boundary, but instead grew around the periphery of the aggregates (Figures 5C and 5F). In addition, when PC dendrites did cross the Slit-expressing boundary, the mean maximum invasion distance of the dendrites was significantly lower than in control conditions (Figure 5G). This repulsive effect is Robo2-dependent, as PC dendrites in explants collected from PC-specific Robo2 deletion animals (*Pcp2-Cre;Robo2*$^{flox/flox}$) showed similar crossing behaviors at both control and Slit-expressing boundaries (Figures 5D–5G). These results demonstrate that Slit-repulsion can prevent dendrite crossing, perhaps mimicking the barrier function of sister dendrites for self-avoidance in vivo.

A Membrane-Localized Slit2 Activity Rescues the Self-Avoidance Defect in Slit2 Mutant PCs

We next asked whether Slit2 activity needs to be localized to the vicinity of PC dendrites, as Slit2 is a secreted molecule but current models of self-avoidance are based on contact-dependent interactions between branches (Grueber and Sagasti, 2010). We designed a rescue experiment with a Slit2 fragment consisting of the second leucine-rich repeat (LRR), termed D2. This fragment was shown to bind to Robos and retain the Slit2 repulsive activity (Hussain et al., 2006) and is small enough to fit in rAAV8.

We performed the rescue experiments in *Pcp2-Cre;Slit2*$^{flox/flox}$ mice using AAV-DsRed (control) and rAAV coexpressing the D2 fragment and GFP (rescue). We expressed one of two forms of D2: a diffusible form termed Slit2D2 and a membrane-bound form termed Slit2D2GPI, which utilizes a glycosylphosphatidylinositol (GPI) anchor (Figure 6A). As labeled by control AAV-DsRed, Slit2-deficient PCs (Figures 6B–6D and 6K) exhibited a high frequency of self-crossing (5.7 ± 0.4/100 μm) at a level comparable to that of single *Slit2* mutant PCs described above (Figure 6K versus Figure 4J). Surprisingly, PCs infected with AAV-Slit2D2-GFP (Figures 6E–6G and 6K) showed a similar defect (5.4 ± 1.0/100 μm), suggesting that the diffusible form is insufficient to rescue the defect. Interestingly, the frequency of self-crossing was dramatically decreased (1.8 ± 0.3/100 μm) in PCs infected with AAV-Slit2D2GPI-GFP that expressed the membrane-bound D2 fragment (Figures 6H–6K). Because the GPI anchor tethers the D2 fragment to the plasma membrane (Figure S4), the rescue by Slit2D2GPI suggests an important role of localized Slit2 activity in preventing self-crossing of PC dendrites (Figure 6L).

Slit/Robo and Pcdhgs Independently Mediate Self-Avoidance at the PC Dendrite Surface

Recent work has demonstrated the role of Pcdhgs in mediating PC dendrite self-avoidance (Lefebvre et al., 2012), providing us an opportunity to test whether the two molecular pathways act in a linear fashion or separately (Model 1 and 2 in Figure 7A). Two experiments were carried out using a *Pcdhg*^{fcon3} allele that has the common intracellular region deleted (Lefebvre et al., 2008).

First, we performed a rescue experiment by injecting *Pcdhg*$^{fcon3/fcon3}$ neonatal pups with two AAVs, one coexpressing Cre and a mCherry marker while another coexpressing Slit2D2GPI and a GFP marker. We analyzed PCs coinfected with both AAVs, which represented Slit2D2GPI rescue in the *Pcdhg* mutant background (Figures 7D and 7E), and compared them to *Pcdhg* mutant PCs in the littermates injected with AAV-Cre-GFP only (Figures 7B and 7C). As predicted, *Pcdhg* mutant PCs exhibit a self-avoidance defect comparable to that previously reported (Lefebvre et al., 2012). Interestingly, Slit2D2GPI overexpression failed to rescue this defect, as both Slit2D2GPI rescue and single *Pcdhg* mutant PCs exhibit similar crossing defects (Figure 7J; 4.8 ± 0.4/100 μm versus 5.6 ± 0.4, respectively). As a comparison, the defects are comparable to that of *Robo2* mutant PCs (Figure 7J versus Figure 2J) and ~6-fold higher than the control cells described above (Figure 2J) or the *Pcdhg*$^{fcon3/fcon3}$*;Robo2*$^{flox/flox}$ control cells infected with AAV-DsRed (Figures 7F, 7G, and 7J; 0.9 ± 0.1/100 μm). This result shows that localized Slit2 activity cannot bypass the requirement of Pcdhg-mediated recognition in self-avoidance and suggests that the two extracellular pathways act separately at the extracellular surface.

This conclusion is further supported by the second study of double *Pcdhg* and *Robo2* deletion in PCs. In the *Pcdhg*$^{fcon3/fcon3}$*;Robo2*$^{flox/flox}$ background, AAV-DsRed infected PCs exhibit normal dendrite morphology with a low frequency of self-crossing, whereas AAV-Cre-GFP^{+} PCs (Figures 7H and 7I) exhibited a significantly increased frequency of self-crossing (Figure 7J; 7.7 ± 0.8/100 μm) with reduced spacing between dendritic branches. Notably, the self-avoidance phenotype in these double mutant PCs is stronger than that from either *Pcdhg* (Figure 7J) or *Robo2* (Figure 2J) single mutants, further suggesting

Figure 4. Slit2 Is Required Cell–Autonomously for PC Dendrite Self-Avoidance

(A and B) In situ hybridization of *Slit2* in P14 cerebellum. Arrows indicate PCs. ML, PCL, GCL are shown in (B) for a high-magnification region of the cerebellum. Scale bars represent 50 μm.

(C) Western blots of P14 cerebellar tissue samples probed by antibodies against Slit2 (top panels). Numbers on the left indicate molecular weight in kDa. Note the increased levels of Slit2 proteins in the ML+PCL relative to the GCL as shown by the relative density (R.D.) normalized to α-tubulin (bottom panel). Labels apply to top and bottom panels (Ce, whole cerebellum).

(D–I) *Slit2*$^{flox/flox}$ PCs infected with AAV-DsRed (D–F) or AAV-Cre-GFP (G–I) are shown by z projections of confocal images (D, E, G, and H) or skeletonized reconstructions (F and I). Boxed regions inside the labeled arbors are enlarged and shown in (E), (F), (H), and (I) respectively. Arrows indicate self-crosses. Scale bars represent 20 μm (D and G); 5 μm (E, F, H, and I).

(J) Quantification of the frequency of self-crossing as the number (#, mean ± SEM) of crosses per 100 μm in the labeled PCs above (n = 18 DsRed cells, six mice; n = 12 Cre-GFP cells, four mice). ****p < 0.0001, Student's t test.

See also Figure S3.

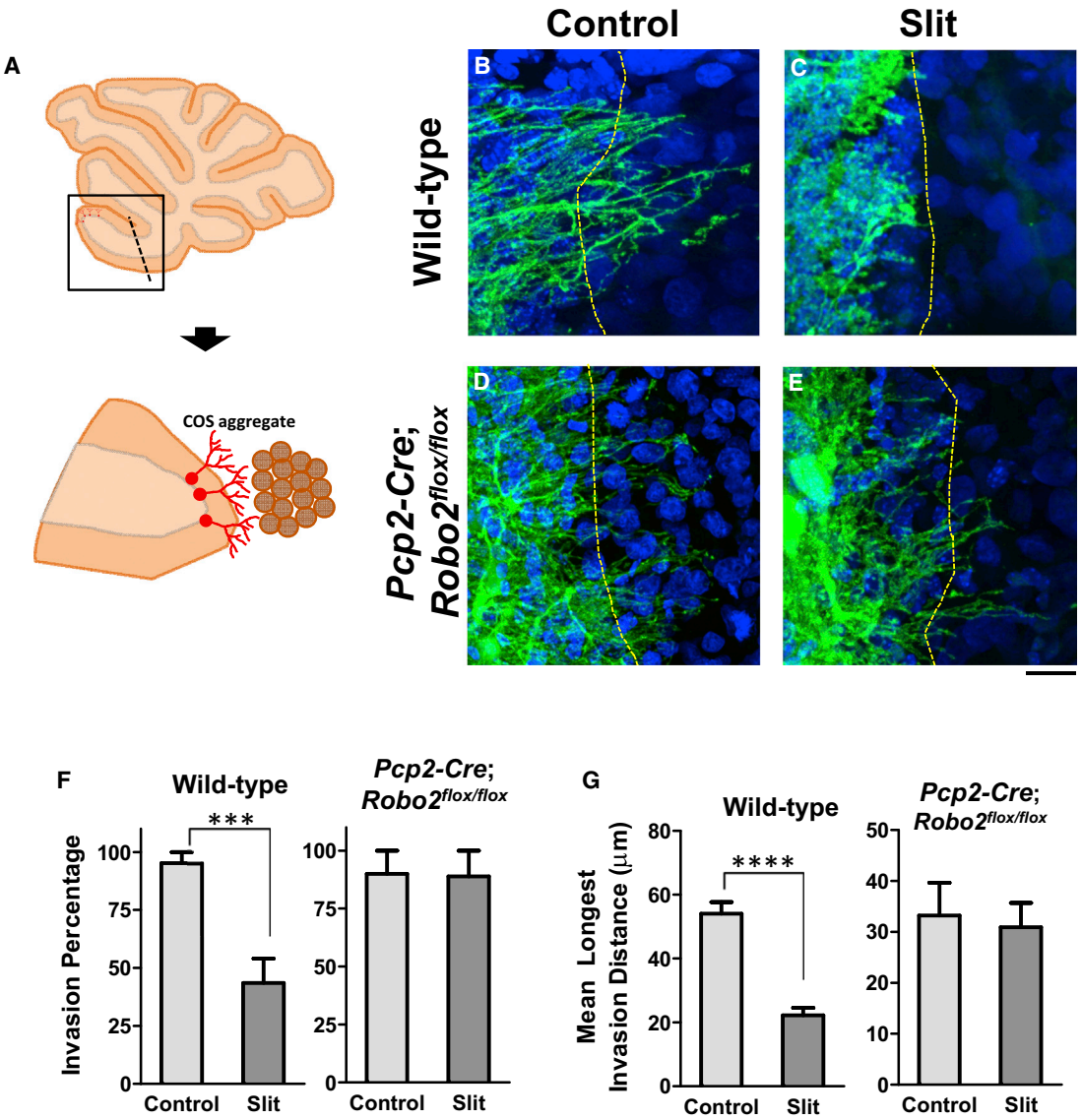

Figure 5. Slits Are Sufficient to Repel PC Dendrites

(A) Schematic illustration of a cerebellar foliar explant isolated from a P7 cerebellum slice and cocultured with a COS cell aggregate when PC dendrites grow away from the explant (brown).

(B–E) Wild-type (B and C) and *Pcp2-Cre;Robo2*$^{flox/flox}$ (D and E) cerebellar explants grown next to control (B and D) or Slit-transfected (C and E) COS cell aggregates were stained for Calbindin-D28k, a marker for PCs and their dendrites; cell nuclei were labeled with Hoechst dye. Dashed lines delineate the explant/aggregate boundary. Scale bars represent 20 μm.

(F and G) Quantification of the percentage of cocultures in which dendrites extended beyond the boundary (F) between wild-type explants (left) and control (n = 21) or Slit-expressing (n = 23) COS aggregates or between *Pcp2-Cre;Robo2*$^{flox/flox}$ explants (right) and control (n = 10) or Slit-expressing (n = 9) COS aggregates. The maximum invasion distances for each condition are shown in (G). Values are expressed by mean ± SEM. ****$p < 0.0001$ and ***$p < 0.001$, Student's t test.

that the two molecules do not act in the same pathway as suggested by Model 1 (Figure 7A). Taken together, these two results strongly favor Model 2 (Figure 7A), in which Pcdhgs and Slit/Robo act separately at the cell surface to mediate PC self-avoidance.

Disrupted Self-Avoidance Is Associated with Gait Alterations in Mice with PC-Specific Robo2 Deletion

Cerebellar PCs are critical to normal motor performance, which can be assayed in a variety of experimental paradigms (Becker et al., 2009; Donald et al., 2008; Li et al., 2010; Sergaki et al., 2010). Because Robo2 can be deleted selectively in all PCs using Pcp2-Cre, we investigated the effects of disrupted dendrite self-avoidance on the motor behavior of *Pcp2-Cre;Robo2*$^{flox/flox}$ mice. These animals retained the self-avoidance phenotype as revealed by single cell analysis (Figure S5A) and showed no obvious locomotor defects under direct observation. We carried out two quantitative assays at P21 for these animals and their littermate controls (*Pcp2-Cre;Robo2*$^{+/+}$): a footprint test to

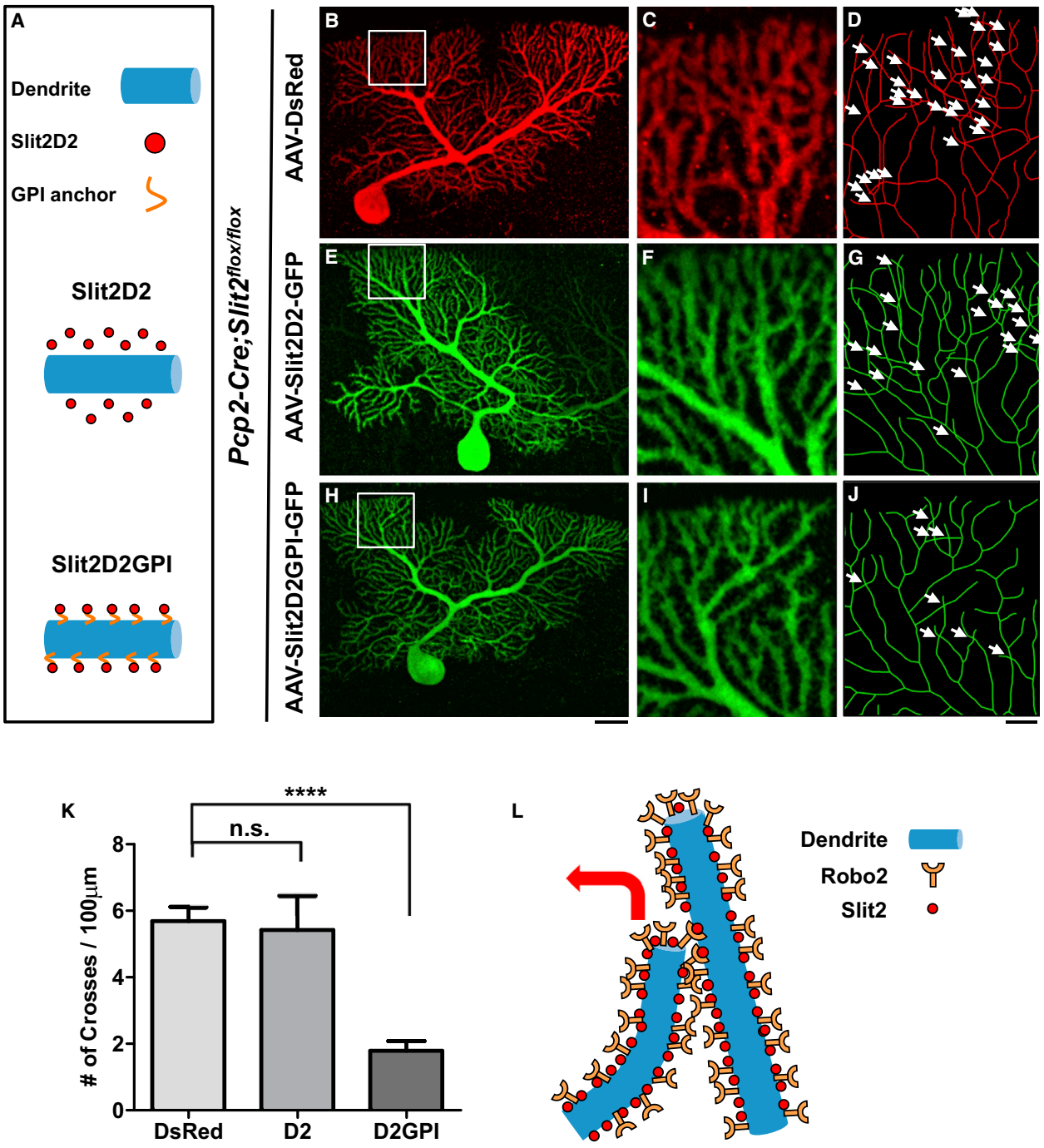

Figure 6. Localizing Slit2 Activity to the Membrane Rescues the Self-Avoidance Defect

(A) Schematic illustration of the constructs expressed in the rescue experiment, including nonlocalized secreted Slit2D2 (middle panel) and membrane-bound Slit2D2GPI (bottom panel).

(B–J) Confocal analysis of *Pcp2-Cre;Slit2*$^{flox/flox}$ PCs infected with either AAV-DsRed (B–D), AAV-GFP-Slit2D2 (E–G), or AAV-GFP-Slit2D2GPI (H–J). Confocal z projections of the entire arbor are shown in (B), (E), and (H), respectively. High-magnification images shown by confocal images (C, F, and I) or skeletonized reconstructions (D, G, and J) of the corresponding boxed region highlight the self-crosses (arrows) in different conditions. Scale bars represent 20 μm (B, E, and H); 5 μm (C, D, F, G, I, and J).

(K) Quantification of the frequency of self-crossing (#/100 μm, mean ± SEM) from the above rescue experiments (n = 6 cells, three mice for all conditions). ****$p < 0.0001$ and n.s., not significant from ANOVA with a Bonferroni post hoc test.

(L) Schematic model illustrating the repulsion of sister branches mediated by membrane-localized Slit2 and its activation of Robo2.

See also Figure S4.

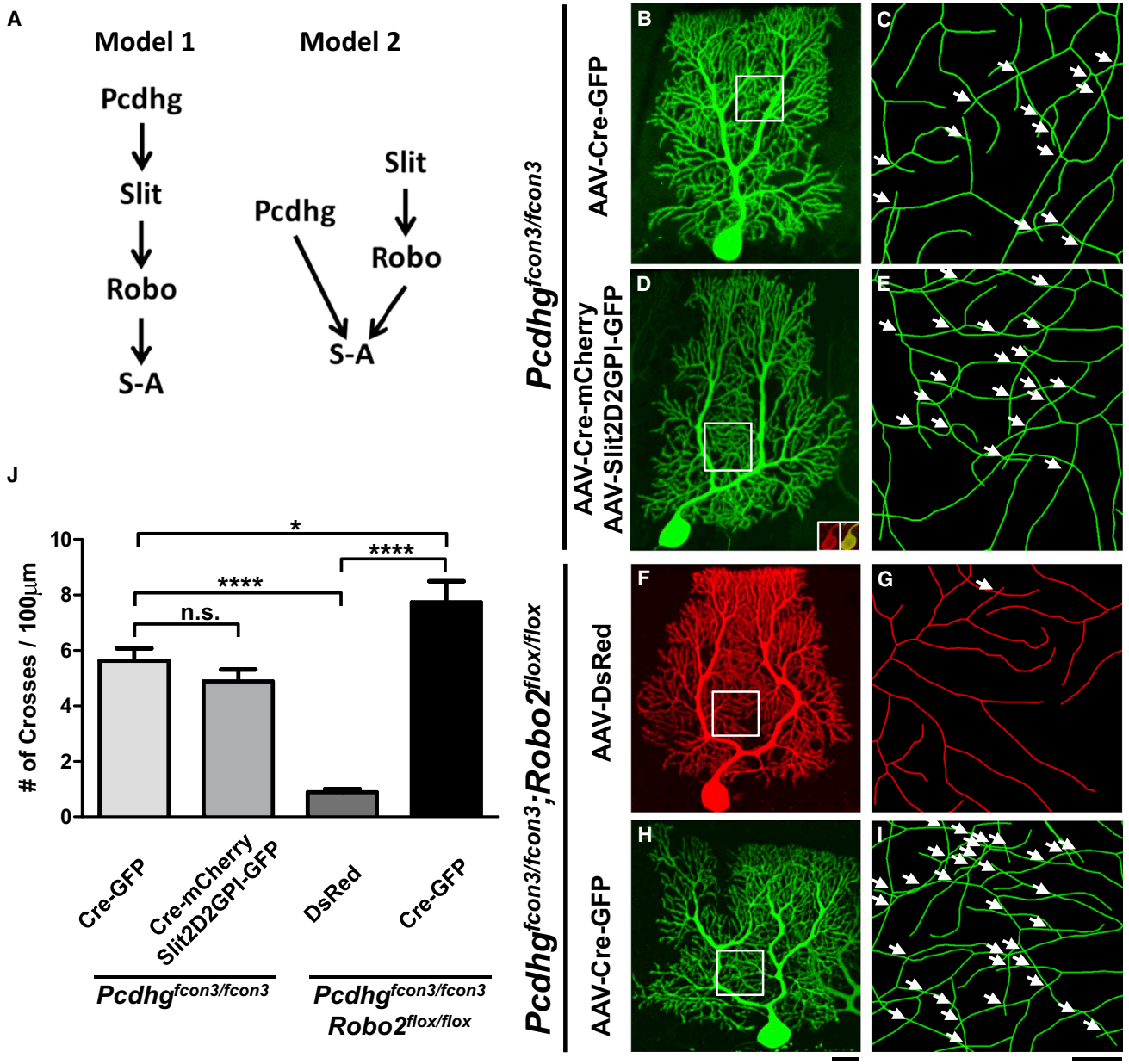

Figure 7. Independent Role of Slit/Robo and Pcdhg Signaling in PC Self-Avoidance

(A) Two models of Slit/Robo and Pcdhg interactions in self-avoidance (S-A): linear signaling (Model 1) versus parallel signaling (Model 2).

(B–E) Confocal analysis of *Pcdhg*$^{fcon3/fcon3}$ PCs infected with AAV-Cre-GFP (B and C) or coinfected with AAV-Cre-mCherry and AAV-Slit2D2GPI-GFP (D and E). Confocal z projections of the entire arbor are shown in (B) and (D). Skeletonized reconstructions (C and E) of the corresponding boxed region highlight the self-crosses (arrows). Insets in (D) show the expression of AAV-Cre-mCherry (red) colocalized with that of AAV-Cre-GFP in the soma.

(F–I) Confocal analysis of *Pcdhg*$^{fcon3/fcon3}$;*Robo2*$^{flox/flox}$ PCs infected with AAV-DsRed (F and G) or AAV-Cre-GFP (H and I). Confocal z projections of the entire arbor are shown in (F) and (H). Skeletonized reconstructions (G and I) of the corresponding boxed region show the self-crosses (arrows).

(J) Quantification of the frequency of self-crossing (#/100 μm, mean ± SEM) in PCs from the above rescue and genetic experiments (n = 8–9 cells, three mice for all conditions). ****$p < 0.0001$, *$p < 0.05$ and n.s., not significant from one-way ANOVA with a Bonferroni post hoc test.

Scale bars represent 20 μm (B, D, F, and H); 5 μm (C, E, G, and I).

examine gait parameters and a dowel rod test for motor coordination and balance (Crawley, 2007).

The footprint test revealed a number of differences between control and mutant mice during locomotion (Figure 8A). First, control animals normally have a strong tendency to place their hindpaw where the forepaw of the same side was previously placed, producing a small distance of "print separation." However, mutant animals showed a large increase in print separation, revealing an irregular pattern of paw placement during normal locomotion (Figure 8B). Second, mutant animals showed a

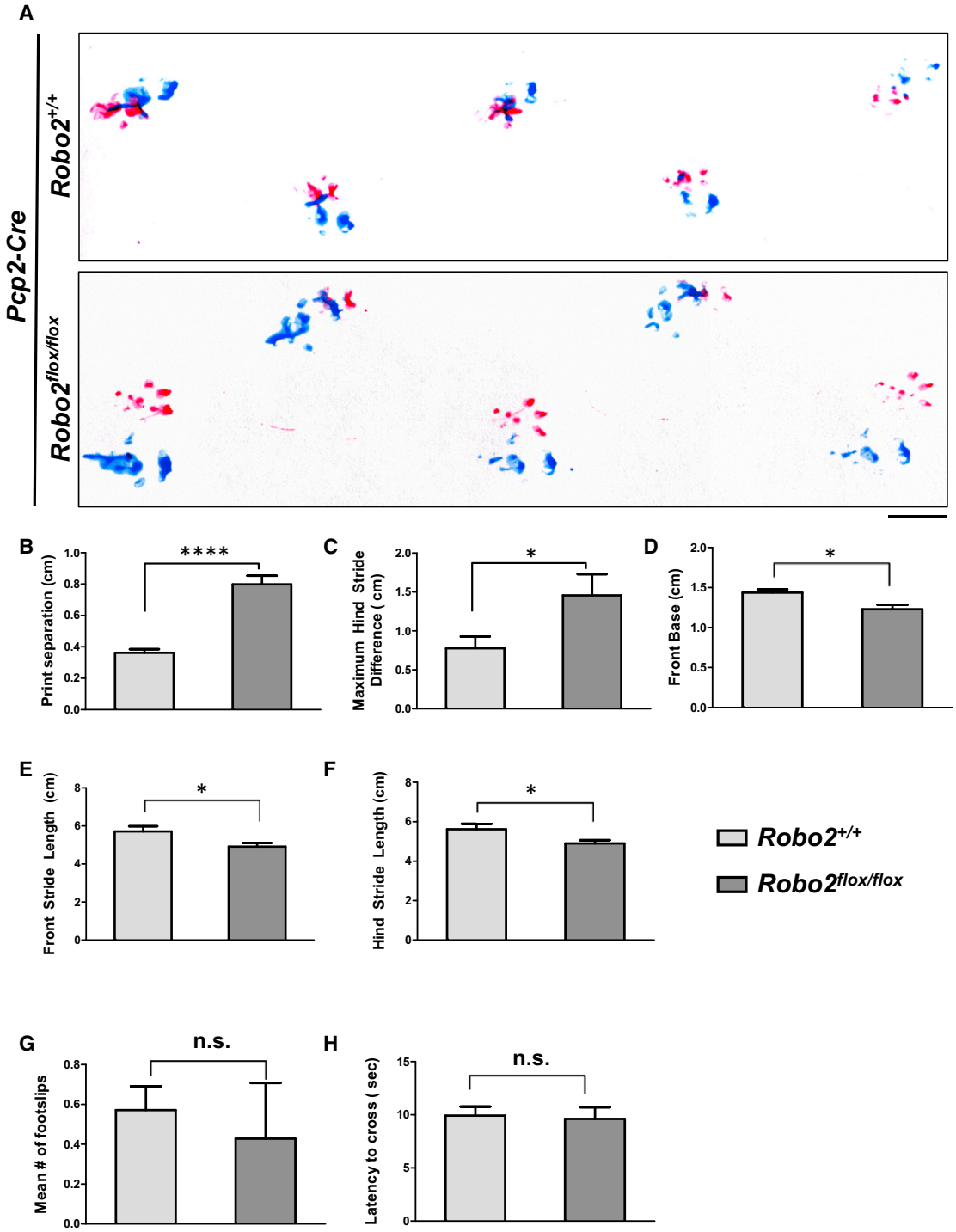

Figure 8. PC-Specific Deletion of Robo2 Is Associated with Gait Alterations

(A) Representative footprint patterns from the gait analysis of *Pcp2-Cre;Robo2*$^{+/+}$ (top) and *Pcp2-Cre;Robo2*$^{flox/flox}$ (bottom) animals (n = 7 animals per genotype). Scale bar represents 1 cm.

(B–F) *Pcp2-Cre;Robo2*$^{flox/flox}$ animals exhibit a number of gait alterations relative to control *Pcp2-Cre;Robo2*$^{+/+}$ littermates, including increased print separation distance (B), increased maximum hind stride difference (C), a narrower front base width (D), and decreased frontpaw (E) and hindpaw (F) stride lengths.

(G–H) Results of the dowel rod test for motor coordination and balance in *Pcp2-Cre;Robo2*$^{+/+}$ and *Pcp2-Cre;Robo2*$^{flox/flox}$ animals, which showed no differences in the mean number of foot slips while crossing (G) or the latency to cross the beam (H).

Values are expressed by mean ± SEM. *p < 0.05, ****p < 0.0001, Student's t test. See also Figure S5.

greater maximum hind stride difference, a measure of stride variability in consecutive steps (Figure 8C). Third, mutant animals exhibited small yet significant changes in several other gait parameters relative to controls, including a smaller front base width (Figure 8D) as well as reduced stride lengths for both front and hind limbs (Figures 8E and 8F). In contrast, the dowel rod test failed to detect any significant differences between control and mutant animals, as both groups crossed the beam with minimal foot slips (Figure 8G) and comparable latencies (Figure 8H). Together, these results suggest that disrupted PC self-avoidance is associated with alterations in a subset of motor behaviors.

To determine whether disrupted self-avoidance altered aspects of synaptic development that could contribute to the observed behavioral changes, we analyzed the cerebellum collected from the same animals used in the motor assays. First, they were costained with antibodies for the PC marker Calbindin-D28k and the presynaptic marker VGLUT1 or VGLUT2 that are associated with parallel fibers (PFs) (Figures S5F and S5G) or climbing fibers (CFs) (Figures S5I and S5J), respectively. Both markers showed similar numbers and distributions in control and mutant animals (Figures S5B–S5D), suggesting that these synapses developed normally. This conclusion is supported by the similar dendritic spine numbers or distribution in AAV-labeled control and mutant PCs (Figures S5L and S5M). Last, mutant animals showed no changes in either the number of PCs (Figures S5E and S5H) or the target of their axonal projections in the deep cerebellar nuclei (Figures S5H–S5K).

DISCUSSION

Self-avoidance is a critical process in patterning neural circuits during development. Here, we demonstrate a role of a classic axon guidance system in regulating this process. We provide genetic evidence to show that the secreted molecule Slit2 and its receptor Robo2 are both required cell-autonomously for creating the nonoverlapping pattern of PC dendrites. Furthermore, we demonstrate that Slit2 has the ability to create a boundary to prevent PC dendrite crossing and the localization of such activity to the membrane is critical in rescuing disrupted self-avoidance. We also show genetically that Slit/Robo and Pcdhg signaling function as separate extracellular pathways to mediate PC self-avoidance. Finally, we provide evidence to link the disruption of PC dendrite self-avoidance to changes in motor behavior.

Both Slit2 and Robo2 Are Required Cell-Autonomously for PC Dendrite Self-Avoidance

The patterning of dendritic arbors by self-avoidance is thought to be mediated by cell-autonomous mechanisms (Grueber and Sagasti, 2010). The strong expression of both *Slit2* and *Robo2* in PCs makes them good candidates for this function, especially as this ligand/receptor pair is known to be involved in repulsive actions of many developmental processes, such as axon guidance and cell migration. Our study using AAV-delivered Cre to delete either gene specifically in PCs provides strong genetic evidence to support this hypothesis. Furthermore, the mosaic approach used in isolated PCs avoids any complications of deleting these genes from neighboring cells. Therefore, our data provide conclusive evidence to demonstrate the cell-autonomous requirement of both Slit2 and Robo2 for proper patterning of PC dendrites.

Our detailed characterization of the phenotype further supports an active role of Slit/Robo signaling in self-avoidance. First, the self-crossing defect found in *Robo2* mutant PCs appears to be independent of the arbor size, shape, and location, but increases in severity along with rising dendritic density, in contrast to normal PCs with intact self-avoidance mechanisms. Second, the defect is related to the loss of an interbranch spacing mechanism, which is not only reflected by 2D crossing in the x-y plane but also manifested by the shortened distance in the z axis. Also, the phenotype is seen during arbor elaboration between P14 and P60, consistent with the effect on distal spiny dendrites but not the primary dendrites. Finally, loss of Slit/Robo signaling appears to only affect dendritic spacing, a key outcome of self-avoidance, as further characterization has not revealed other arbor defects. Thus, our analysis of the phenotypes provides strong support of the function of this extracellular pathway in self-avoidance.

A feature related to self-avoidance is interneuronal tiling, which includes both homotypic and heterotypic interactions (Grueber and Sagasti, 2010). While the PC-specific expression of Slit2 and Robo2 may function in preventing PC dendrites from inappropriately avoiding neighboring non-PCs, it is not currently known from the literature if dendrites from neighboring PCs tile with each other. Our preliminary observations suggest that wild-type PCs do not tile along the entire border of their arbors, but instead exhibit rare instances of small arbor portions that intercalate and tile with each other. We observe this arrangement between pairs of both wild-type and Robo2 mutant PCs (data not shown), suggesting that Slit/Robo signaling may not participate in this particular arrangement of tiling, though it will be of great interest to identify the factors mediating this interneuronal interaction. Furthermore, Slit/Robo signaling is not involved in monoplanar development, which was recently shown to be influenced by neuronal connectivity (Kaneko et al., 2011).

Local Repulsive Action of Slit2 in Dendrite Self-Avoidance

Given that Slit/Robo signaling lacks the molecular diversity to specify the identity of each neuron, the self-avoidance phenotype associated with its loss in PCs suggests that it may mediate a general branch repulsion mechanism instead of self-recognition. This proposed repulsive role is supported by the cerebellar folium coculture assay we developed. Using this assay, we found an inhibitory effect of Slits on PC dendrites that is different from that of the traditionally defined repulsive activity in culture. Unlike secreted semaphorins that can steer neurites away from a distance (Messersmith et al., 1995), Slits exert their inhibitory action only for PC dendrites in the vicinity of the protein source. This local activity is consistent with the boundary-establishing function of Slit/Robo signaling in other developmental processes (Domyan et al., 2013; Ma and Tessier-Lavigne, 2007; Plump et al., 2002; Wang et al., 2013).

The boundary establishing activity of Slit is also consistent with the requirement of local repulsion in self-avoidance, a

conclusion that is supported by the rescue experiment, in which only membrane-associated Slit2 activity is capable of correcting the self-crossing defects in *Slit2* mutant PCs. Although the rescue experiment only demonstrates where the repulsive activity is needed, the notion that the native proteins act in a localized fashion is consistent with the physical properties of Slit proteins, which are known to be cleaved and associate with cell membranes (Nguyen-Ba-Charvet et al., 2001; Wang et al., 1999). Additionally, recent studies have shown that Slit can interact with and be localized by extracellular matrix (ECM) components, such as dystroglycan (Wright et al., 2012) and collagen (Xiao et al., 2011). Thus, it is possible that secreted Slit proteins are anchored either on the dendritic membrane or nearby in the ECM to create a repulsive boundary for neighboring branches. This hypothesis is also consistent with the recent discovery of the interaction between dendrites and neighboring tissues via an extracellular molecular adhesion complex (Dong et al., 2013; Salzberg et al., 2013).

The cell-autonomous function described here for Slit2 is distinct from Netrin, another secreted cue that was implicated in dendrite self-avoidance in *C. elegans* (Smith et al., 2012). There, Netrin does not act cell-autonomously, but instead diffuses into the extracellular space where it is captured by its Unc40 receptor on the dendrite and then presented to the Unc5 receptor of the neighboring dendrite, both of which contact each other in a head-on fashion. This unique action for a secreted molecule may reflect a fundamental difference in the mechanisms of self-avoidance between dendritic arbors of different geometries. Taken together, our study points to the different means by which secreted molecules pattern dendritic arbors.

Two Independent Pathways Mediate PC dendrite Self-Avoidance at the Cell Surface

Combined with the recent discovery of Pcdhg-mediated self-recognition in PCs (Lefebvre et al., 2012), our study demonstrates the presence of a second molecular pathway that is required for self-avoidance in the same cell type. We investigated any putative in vivo interactions between these two signaling systems and considered two general models by which Pcdhgs and Slit/Robo might function in self-avoidance. The first model positions Pcdhgs and Slit/Robo in a linear pathway, starting with Pcdhg-mediated recognition that is followed by Slit/Robo-mediated sister branch repulsion. The second model posits that the two pathways act in parallel at the cell surface, with Pcdhgs mediating recognition-dependent self-avoidance and Slit/Robo mediating a more general, likely recognition-independent repulsive function.

The failure of Slit2D2GPI to rescue the self-avoidance defect in *Pcdhg* mutant PCs and the aggravated phenotype in *Pcdhg/Robo2* double mutant PCs argues against the first model of a shared pathway. If Pcdhg-mediated recognition results in Slit/Robo-mediated branch repulsion in vivo, then direct activation of the Slit/Robo pathway via overexpression of the membrane-bound Slit2 fragment (Slit2D2GPI) should bypass the requirement of Pcdhg signaling. Instead, Slit2D2GPI overexpression failed to rescue the defect, indicating that Slit/Robo does not act downstream of Pcdhgs. Additionally, if Pcdhgs and Slit/Robo act in the same linear pathway, then double *Pcdhg/Robo2* mutant PCs would be expected to have a phenotype similar to either single mutant. In contrast, *Pcdhg/Robo2* double mutants exhibit an aggravated phenotype. Taken together, these two results support the idea that Pcdhgs and Slit/Robo act in parallel to promote PC dendrite self-avoidance. Lastly, we observe no appreciable qualitative differences between the *Slit/Robo* and *Pcdhg* mutant phenotypes, suggesting that Slit/Robo specifically mediates self-avoidance, as opposed to different functions with a similar outcome.

The presence of multiple self-avoidance mechanisms in a single cell is not without precedent, as the class IV da neurons in *Drosophila* use mechanisms in addition to Dscam-mediated recognition (Long et al., 2009; Matsubara et al., 2011). This may be an effective strategy for ensuring that each dendrite occupies a discrete spatial domain, which can be achieved by converging onto common intracellular components. Because little is known about the intracellular mechanisms for self-avoidance, it will be of great interest to test the role of those components identified for Slit/Robo repulsion in PC self-avoidance (Bashaw and Klein, 2010; O'Donnell et al., 2009) and determine their requirement for both pathways.

Motor Behavior of Self-Avoidance Mutants

Despite the recent success in identifying the molecular mechanisms of self-avoidance in a number of cell types, little is known about the consequences of disrupting this widely seen patterning feature for circuit function or animal behavior. The extensively branched PC dendritic arbor is critical for integrating a large number of diverse synaptic inputs (Häusser et al., 2000) and hence normal motor behavior (Becker et al., 2009; Donald et al., 2008; Li et al., 2010; Sergaki et al., 2010). Taking advantage of this function, we used behavioral assays to demonstrate the effect of disrupted self-avoidance on motor circuit function. In particular, we show that population-wide deletion of Robo2 in PCs is associated with gait alterations, specifically an irregular pattern of paw placement, without affecting general synaptic development.

How might a disruption of self-avoidance produce a change in motor behavior? Interestingly, the self-avoidance defect only affects the spiny distal branches that synapse with PFs, but not the CF-innervated smooth primary dendrites, suggesting that a change in PF-PC connectivity could underlie the observed motor deficits, as previously shown by mutating the glutamate receptor (Kashiwabuchi et al., 1995). While our analysis of both pre- and postsynaptic elements suggests overall normal development, we cannot exclude the possibility of nonmorphological changes in PF-PC connectivity, perhaps by altering synapse distribution across branches or their transmission properties. Further investigation by electron microscopy and electrophysiology will be necessary to determine the consequences of self-avoidance defects on synaptic functions. Additionally, the self-avoidance defect may alter interactions between PCs and interneurons in the ML. Regardless, cerebellar PCs provide an accessible system to further address these questions and understand the role of dendrite organization in neural circuit function that is critical to behavior.

In summary, our discovery of a second pathway mediating PC self-avoidance highlights the importance and complexity of

local molecular interactions during dendritic development (Jan and Jan, 2010). Furthermore, our elucidation of a role for a canonical repulsive guidance cue in self-avoidance has general implications for understanding molecular regulation of dendritic patterning during neural circuit assembly (Zipursky and Sanes, 2010). Finally, our observation of behavioral changes associated with self-avoidance defects suggests potential contributions of dendritic patterning to circuit functions, a connection that warrants further investigation in the future.

EXPERIMENTAL PROCEDURES

Mouse Strains

The *Robo2*^{flox} and *Pcdhg*^{fcon3} conditional alleles and the PC-specific *Pcp2-Cre* driver were described previously (Barski et al., 2000; Lefebvre et al., 2008; Lu et al., 2007). The *Slit2*^{flox} conditional allele containing loxP sequences flanking exon 8 was established at the MCI/ICS (Mouse Clinical Institute, Institut Clinique de la Souris, Illkirch, France; http://www.ics-mci.fr/). Cre-dependent deletion interrupts Slit2 proteins after Thr203 located in the first LRR. All mice were maintained in a mixed C57BL6/CD-1 background and used in accordance with protocols approved by the Institutional Animal Care and Use Committees at the University of Southern California following National Health Institutes (NIH) regulations.

Expression Analysis by In Situ Hybridization, Immunohistochemistry, and Western Blot

In situ analysis (Zhao and Ma, 2009) was done in P14 cerebellar sections using digoxigenin (DIG)-labeled RNA probes for Slits and Robos (Brose et al., 1999). Robo2 staining was done in P21 cerebellar sections (16 μm). Western blots were done with protein extracts of whole cerebellar, dissected GCL, or ML+PCL tissues from P14 animals.

Analysis of PC Dendrites after AAV Injection

rAAVs produced by Vector BioLabs were injected into P0 newborn mouse pups as previously described (Gibson and Ma, 2011). P14-P60 cerebella were sectioned (100 or 16 μm) and immunostained. Labeled PC dendrites were stained with anti-GFP (Aves Labs) or anti-DsRed (Clontech) antibodies followed by Cy2- or Cy3-conjugated secondary antibodies (Jackson ImmunoResearch). Optical sections were collected on a confocal microscope (LSM5; Zeiss) and analyzed using Neurolucida (MBF Bioscience). Any two branches crossing over each other were marked and counted manually in z projections. Neurolucida Explorer was used to calculate total dendrite area, number of dendritic branches, and dendrite length. The z distance between crossing branches was calculated from 3D reconstructions.

The sampling method was based on grids of 10 × 10 μm squares overlaid on top of the z projection of PC confocal stacks (Figure S2A). A minimum of 20% of all grid squares covering the entire tree were randomly selected for 3D reconstruction (Figure S2B) and further analysis of self-crossing frequencies, separation between crossing branches along the z axis, and the relationship between dendrite density and the number of self-crosses. It was validated against full reconstructions to detect differences between different genotypes (Figures S2C and S2D).

PC Explant Cocultures

Foliar explants isolated from P7 coronal cerebellar sections were placed on cell-culture inserts (0.4 μm; Millipore) floating on top of culture media. Fifty percent media was replenished every 3 days. COS cell aggregates prepared via the hanging drop method (Kennedy et al., 1994) were placed adjacent to the explants after 10 DIV, and the explants were analyzed by immunostaining after an additional 3 DIV.

Behavioral Assays

All behavioral assays were performed at P21. Gait analysis was performed using a footprint test and motor coordination/balance was assayed using a dowel rod test. The experimenter performing the assays was blind to the genotype throughout data acquisition.

Statistics

Comparisons of two samples were done by Student's t test, with Welch's correction for unequal variances when appropriate. Multiple comparisons were made by one-way ANOVA with a Bonferroni post hoc test.

SUPPLEMENTAL INFORMATION

Supplemental Information includes Supplemental Experimental Procedures and five figures and can be found with this article online at http://dx.doi.org/10.1016/j.neuron.2014.01.009.

ACKNOWLEDGMENTS

We thank members of the Ma lab for discussion, N. Renier for sharing antibody testing results, B. Thompson and D. Campbell for help with the gait analysis, the Jakowec lab for help with the dowel rod test, and the Levitt lab for advice on the behavioral assays. We thank King's College London for sharing the *Robo2*$^{flox/flox}$ mouse and W. Lu for sending the mouse. We also thank D. Ginty, L. Lillien, and D. Miller for comments on the early version of the manuscript. This work was supported by grants from the National Health Institutes (NIH) (NS062047 to L.M.; EY022073 to J.R.S.), Fondation pour la Recherche Médicale and the French State program "Investissements d'Avenir" managed by the Agence Nationale de la Recherche (LIFESENSES: ANR-10-LABX-65) (to A.C.), and the Wright Foundation (to L.M.).

Accepted: December 23, 2013
Published: March 5, 2014

REFERENCES

Baker, M.W., and Macagno, E.R. (2000). The role of a LAR-like receptor tyrosine phosphatase in growth cone collapse and mutual-avoidance by sibling processes. J. Neurobiol. *44*, 194–203.

Barski, J.J., Dethleffsen, K., and Meyer, M. (2000). Cre recombinase expression in cerebellar Purkinje cells. Genesis *28*, 93–98.

Bashaw, G.J., and Klein, R. (2010). Signaling from axon guidance receptors. Cold Spring Harb. Perspect. Biol. *2*, a001941.

Becker, E.B., Oliver, P.L., Glitsch, M.D., Banks, G.T., Achilli, F., Hardy, A., Nolan, P.M., Fisher, E.M., and Davies, K.E. (2009). A point mutation in TRPC3 causes abnormal Purkinje cell development and cerebellar ataxia in moonwalker mice. Proc. Natl. Acad. Sci. USA *106*, 6706–6711.

Borrell, V., Cárdenas, A., Ciceri, G., Galcerán, J., Flames, N., Pla, R., Nóbrega-Pereira, S., García-Frigola, C., Peregrín, S., Zhao, Z., et al. (2012). Slit/Robo signaling modulates the proliferation of central nervous system progenitors. Neuron *76*, 338–352.

Brose, K., Bland, K.S., Wang, K.H., Arnott, D., Henzel, W., Goodman, C.S., Tessier-Lavigne, M., and Kidd, T. (1999). Slit proteins bind Robo receptors and have an evolutionarily conserved role in repulsive axon guidance. Cell *96*, 795–806.

Chédotal, A. (2007). Slits and their receptors. Adv. Exp. Med. Biol. *621*, 65–80.

Chen, W.V., Alvarez, F.J., Lefebvre, J.L., Friedman, B., Nwakeze, C., Geiman, E., Smith, C., Thu, C.A., Tapia, J.C., Tasic, B., et al. (2012). Functional significance of isoform diversification in the protocadherin gamma gene cluster. Neuron *75*, 402–409.

Crawley, J.N. (2007). What's Wrong With My Mouse? Behavioral Phenotyping of Transgenic and Knockout Mice. (New Jersey: John Wiley & Sons).

Domyan, E.T., Branchfield, K., Gibson, D.A., Naiche, L.A., Lewandoski, M., Tessier-Lavigne, M., Ma, L., and Sun, X. (2013). Roundabout receptors are critical for foregut separation from the body wall. Dev. Cell *24*, 52–63.

Donald, S., Humby, T., Fyfe, I., Segonds-Pichon, A., Walker, S.A., Andrews, S.R., Coadwell, W.J., Emson, P., Wilkinson, L.S., and Welch, H.C. (2008).

P-Rex2 regulates Purkinje cell dendrite morphology and motor coordination. Proc. Natl. Acad. Sci. USA *105*, 4483–4488.

Dong, X., Liu, O.W., Howell, A.S., and Shen, K. (2013). An extracellular adhesion molecule complex patterns dendritic branching and morphogenesis. Cell *155*, 296–307.

Fuerst, P.G., Bruce, F., Tian, M., Wei, W., Elstrott, J., Feller, M.B., Erskine, L., Singer, J.H., and Burgess, R.W. (2009). DSCAM and DSCAML1 function in self-avoidance in multiple cell types in the developing mouse retina. Neuron *64*, 484–497.

Fujishima, K., Horie, R., Mochizuki, A., and Kengaku, M. (2012). Principles of branch dynamics governing shape characteristics of cerebellar Purkinje cell dendrites. Development *139*, 3442–3455.

Gibson, D.A., and Ma, L. (2011). Mosaic analysis of gene function in postnatal mouse brain development by using virus-based Cre recombination. J. Vis. Exp. *Aug 1*, http://dx.doi.org/10.3791/2823.

Giovannone, D., Reyes, M., Reyes, R., Correa, L., Martinez, D., Ra, H., Gomez, G., Kaiser, J., Ma, L., Stein, M.-P., and de Bellard, M.E. (2012). Slits affect the timely migration of neural crest cells via Robo receptor. Dev. Dyn. *241*, 1274–1288.

Grieshammer, U., Le Ma, Plump, A.S., Wang, F., Tessier-Lavigne, M., and Martin, G.R. (2004). SLIT2-mediated ROBO2 signaling restricts kidney induction to a single site. Dev. Cell *6*, 709–717.

Grueber, W.B., and Sagasti, A. (2010). Self-avoidance and tiling: mechanisms of dendrite and axon spacing. Cold Spring Harb. Perspect. Biol. *2*, a001750.

Han, C., Wang, D., Soba, P., Zhu, S., Lin, X., Jan, L.Y., and Jan, Y.N. (2012). Integrins regulate repulsion-mediated dendritic patterning of Drosophila sensory neurons by restricting dendrites in a 2D space. Neuron *73*, 64–78.

Häusser, M., Spruston, N., and Stuart, G.J. (2000). Diversity and dynamics of dendritic signaling. Science *290*, 739–744.

Hughes, M.E., Bortnick, R., Tsubouchi, A., Bäumer, P., Kondo, M., Uemura, T., and Schmucker, D. (2007). Homophilic Dscam interactions control complex dendrite morphogenesis. Neuron *54*, 417–427.

Hussain, S.A., Piper, M., Fukuhara, N., Strochlic, L., Cho, G., Howitt, J.A., Ahmed, Y., Powell, A.K., Turnbull, J.E., Holt, C.E., and Hohenester, E. (2006). A molecular mechanism for the heparan sulfate dependence of Slit-Robo signaling. J. Biol. Chem. *281*, 39693–39698.

Jan, Y.N., and Jan, L.Y. (2010). Branching out: mechanisms of dendritic arborization. Nat. Rev. Neurosci. *11*, 316–328.

Kaneko, M., Yamaguchi, K., Eiraku, M., Sato, M., Takata, N., Kiyohara, Y., Mishina, M., Hirase, H., Hashikawa, T., and Kengaku, M. (2011). Remodeling of monoplanar Purkinje cell dendrites during cerebellar circuit formation. PLoS ONE *6*, e20108.

Kashiwabuchi, N., Ikeda, K., Araki, K., Hirano, T., Shibuki, K., Takayama, C., Inoue, Y., Kutsuwada, T., Yagi, T., Kang, Y., et al. (1995). Impairment of motor coordination, Purkinje cell synapse formation, and cerebellar long-term depression in GluR delta 2 mutant mice. Cell *81*, 245–252.

Kennedy, T.E., Serafini, T., de la Torre, J.R., and Tessier-Lavigne, M. (1994). Netrins are diffusible chemotropic factors for commissural axons in the embryonic spinal cord. Cell *78*, 425–435.

Kim, M.E., Shrestha, B.R., Blazeski, R., Mason, C.A., and Grueber, W.B. (2012). Integrins establish dendrite-substrate relationships that promote dendritic self-avoidance and patterning in Drosophila sensory neurons. Neuron *73*, 79–91.

Kramer, A.P., and Kuwada, J.Y. (1983). Formation of the receptive fields of leech mechanosensory neurons during embryonic development. J. Neurosci. *3*, 2474–2486.

Lefebvre, J.L., Zhang, Y., Meister, M., Wang, X., and Sanes, J.R. (2008). gamma-Protocadherins regulate neuronal survival but are dispensable for circuit formation in retina. Development *135*, 4141–4151.

Lefebvre, J.L., Kostadinov, D., Chen, W.V., Maniatis, T., and Sanes, J.R. (2012). Protocadherins mediate dendritic self-avoidance in the mammalian nervous system. Nature *488*, 517–521.

Lein, E.S., Hawrylycz, M.J., Ao, N., Ayres, M., Bensinger, A., Bernard, A., Boe, A.F., Boguski, M.S., Brockway, K.S., Byrnes, E.J., et al. (2007). Genome-wide atlas of gene expression in the adult mouse brain. Nature *445*, 168–176.

Li, J., Gu, X., Ma, Y., Calicchio, M.L., Kong, D., Teng, Y.D., Yu, L., Crain, A.M., Vartanian, T.K., Pasqualini, R., et al. (2010). Nna1 mediates Purkinje cell dendritic development via lysyl oxidase propeptide and NF-κB signaling. Neuron *68*, 45–60.

Liu, Y., and Halloran, M.C. (2005). Central and peripheral axon branches from one neuron are guided differentially by Semaphorin3D and transient axonal glycoprotein-1. J. Neurosci. *25*, 10556–10563.

Long, H., Sabatier, C., Ma, L., Plump, A., Yuan, W., Ornitz, D.M., Tamada, A., Murakami, F., Goodman, C.S., and Tessier-Lavigne, M. (2004). Conserved roles for Slit and Robo proteins in midline commissural axon guidance. Neuron *42*, 213–223.

Long, H., Ou, Y., Rao, Y., and van Meyel, D.J. (2009). Dendrite branching and self-avoidance are controlled by Turtle, a conserved IgSF protein in Drosophila. Development *136*, 3475–3484.

Lu, W., van Eerde, A.M., Fan, X., Quintero-Rivera, F., Kulkarni, S., Ferguson, H., Kim, H.G., Fan, Y., Xi, Q., Li, Q.G., et al. (2007). Disruption of ROBO2 is associated with urinary tract anomalies and confers risk of vesicoureteral reflux. Am. J. Hum. Genet. *80*, 616–632.

Ma, L., and Tessier-Lavigne, M. (2007). Dual branch-promoting and branch-repelling actions of Slit/Robo signaling on peripheral and central branches of developing sensory axons. J. Neurosci. *27*, 6843–6851.

Marillat, V., Cases, O., Nguyen-Ba-Charvet, K.T., Tessier-Lavigne, M., Sotelo, C., and Chédotal, A. (2002). Spatiotemporal expression patterns of slit and robo genes in the rat brain. J. Comp. Neurol. *442*, 130–155.

Matsubara, D., Horiuchi, S.Y., Shimono, K., Usui, T., and Uemura, T. (2011). The seven-pass transmembrane cadherin Flamingo controls dendritic self-avoidance via its binding to a LIM domain protein, Espinas, in Drosophila sensory neurons. Genes Dev. *25*, 1982–1996.

Matsuoka, R.L., Jiang, Z., Samuels, I.S., Nguyen-Ba-Charvet, K.T., Sun, L.O., Peachey, N.S., Chedotal, A., Yau, K.W., and Kolodkin, A.L. (2012). Guidance-cue control of horizontal cell morphology, lamination, and synapse formation in the mammalian outer retina. J. Neurosci. *32*, 6859–6868.

Matthews, B.J., Kim, M.E., Flanagan, J.J., Hattori, D., Clemens, J.C., Zipursky, S.L., and Grueber, W.B. (2007). Dendrite self-avoidance is controlled by Dscam. Cell *129*, 593–604.

McKay, B.E., and Turner, R.W. (2005). Physiological and morphological development of the rat cerebellar Purkinje cell. J. Physiol. *567*, 829–850.

Messersmith, E.K., Leonardo, E.D., Shatz, C.J., Tessier-Lavigne, M., Goodman, C.S., and Kolodkin, A.L. (1995). Semaphorin III can function as a selective chemorepellent to pattern sensory projections in the spinal cord. Neuron *14*, 949–959.

Montague, P.R., and Friedlander, M.J. (1991). Morphogenesis and territorial coverage by isolated mammalian retinal ganglion cells. J. Neurosci. *11*, 1440–1457.

Nguyen-Ba-Charvet, K.T., Brose, K., Marillat, V., Sotelo, C., Tessier-Lavigne, M., and Chédotal, A. (2001). Sensory axon response to substrate-bound Slit2 is modulated by laminin and cyclic GMP. Mol. Cell. Neurosci. *17*, 1048–1058.

O'Donnell, M., Chance, R.K., and Bashaw, G.J. (2009). Axon growth and guidance: receptor regulation and signal transduction. Annu. Rev. Neurosci. *32*, 383–412.

Pilpel, N., Landeck, N., Klugmann, M., Seeburg, P.H., and Schwarz, M.K. (2009). Rapid, reproducible transduction of select forebrain regions by targeted recombinant virus injection into the neonatal mouse brain. J. Neurosci. Methods *182*, 55–63.

Plump, A.S., Erskine, L., Sabatier, C., Brose, K., Epstein, C.J., Goodman, C.S., Mason, C.A., and Tessier-Lavigne, M. (2002). Slit1 and Slit2 cooperate to prevent premature midline crossing of retinal axons in the mouse visual system. Neuron *33*, 219–232.

Sagasti, A., Guido, M.R., Raible, D.W., and Schier, A.F. (2005). Repulsive interactions shape the morphologies and functional arrangement of zebrafish peripheral sensory arbors. Curr. Biol. *15*, 804–814.

Salzberg, Y., Díaz-Balzac, C.A., Ramirez-Suarez, N.J., Attreed, M., Tecle, E., Desbois, M., Kaprielian, Z., and Bülow, H.E. (2013). Skin-derived cues control arborization of sensory dendrites in Caenorhabditis elegans. Cell *155*, 308–320.

Sdrulla, A.D., and Linden, D.J. (2006). Dynamic imaging of cerebellar Purkinje cells reveals a population of filopodia which cross-link dendrites during early postnatal development. Cerebellum *5*, 105–115.

Sergaki, M.C., Guillemot, F., and Matsas, R. (2010). Impaired cerebellar development and deficits in motor coordination in mice lacking the neuronal protein BM88/Cend1. Mol. Cell. Neurosci. *44*, 15–29.

Smith, C.J., Watson, J.D., VanHoven, M.K., Colón-Ramos, D.A., and Miller, D.M., 3rd. (2012). Netrin (UNC-6) mediates dendritic self-avoidance. Nat. Neurosci. *15*, 731–737.

Soba, P., Zhu, S., Emoto, K., Younger, S., Yang, S.J., Yu, H.H., Lee, T., Jan, L.Y., and Jan, Y.N. (2007). Drosophila sensory neurons require Dscam for dendritic self-avoidance and proper dendritic field organization. Neuron *54*, 403–416.

Wang, K.H., Brose, K., Arnott, D., Kidd, T., Goodman, C.S., Henzel, W., and Tessier-Lavigne, M. (1999). Biochemical purification of a mammalian slit protein as a positive regulator of sensory axon elongation and branching. Cell *96*, 771–784.

Wang, S.Z., Ibrahim, L.A., Kim, Y.J., Gibson, D.A., Leung, H.C., Yuan, W., Zhang, K.K., Tao, H.W., Ma, L., and Zhang, L.I. (2013). Slit/Robo signaling mediates spatial positioning of spiral ganglion neurons during development of cochlear innervation. J. Neurosci. *33*, 12242–12254.

Wojtowicz, W.M., Flanagan, J.J., Millard, S.S., Zipursky, S.L., and Clemens, J.C. (2004). Alternative splicing of Drosophila Dscam generates axon guidance receptors that exhibit isoform-specific homophilic binding. Cell *118*, 619–633.

Wojtowicz, W.M., Wu, W., Andre, I., Qian, B., Baker, D., and Zipursky, S.L. (2007). A vast repertoire of Dscam binding specificities arises from modular interactions of variable Ig domains. Cell *130*, 1134–1145.

Wright, K.M., Lyon, K.A., Leung, H., Leahy, D.J., Ma, L., and Ginty, D.D. (2012). Dystroglycan organizes axon guidance cue localization and axonal pathfinding. Neuron *76*, 931–944.

Wu, J.Y., Feng, L., Park, H.T., Havlioglu, N., Wen, L., Tang, H., Bacon, K.B., Jiang Zh, Zhang Xc, and Rao, Y. (2001). The neuronal repellent Slit inhibits leukocyte chemotaxis induced by chemotactic factors. Nature *410*, 948–952.

Xiao, T., Staub, W., Robles, E., Gosse, N.J., Cole, G.J., and Baier, H. (2011). Assembly of lamina-specific neuronal connections by slit bound to type IV collagen. Cell *146*, 164–176.

Yagi, T. (2008). Clustered protocadherin family. Dev. Growth Differ. *50* (*Suppl 1*), S131–S140.

Zhao, Z., and Ma, L. (2009). Regulation of axonal development by natriuretic peptide hormones. Proc. Natl. Acad. Sci. USA *106*, 18016–18021.

Zipursky, S.L., and Sanes, J.R. (2010). Chemoaffinity revisited: dscams, protocadherins, and neural circuit assembly. Cell *143*, 343–353.